

DOI: 10.1002/chem.201302100

# Remarkable Regioisomer Control in the Hydrogel Formation from a Two-Component Mixture of Pyridine-End Oligo(*p*-phenylenevinylene)s and *N*-Decanoyl-L-alanine

Subham Bhattacharjee,<sup>[a]</sup> Sougata Datta,<sup>[a]</sup> and Santanu Bhattacharya\*<sup>[a, b]</sup>

**Abstract:** *N*-Decanoyl-L-alanine (DA) was mixed with either colorless 4,4'-bipyridine (BP) or various derivatives such as chromogenic oligo(*p*-phenylenevinylene) (OPV) functionalized with isomeric pyridine termini in specific molar ratios. This mixtures form salt-type gels in a water/ethanol (2:1, v/v) mixture. The gelation properties of these two-component mixtures could be modulated by variation of the position of the "N" atom of the end pyridyl groups in OPVs. The presence of acid-base interactions in the self-assembly of these two-component systems leading to gelation was probed in detail by using stoichiometry-dependent UV/Vis and FTIR spectroscopy. Furthermore, temperature-dependent UV/Vis and

fluorescence spectroscopy clearly demonstrated a J-type aggregation mode of these gelator molecules during the sol-to-gel transition process. Morphological features and the arrangement of the molecules in the gels were examined by using scanning electron microscopy (SEM), atomic force microscopy (AFM), and X-ray diffraction (XRD) techniques. Calculation of the length of each molecular system by energy minimization in its extended conformation and comparison with the XRD patterns revealed that this class of gelator mole-

cules adopts lamellar organizations. Rheological properties of these two-component systems provided clear evidence that the flow behavior could be modulated by varying the acid/amine ratio. Polarized optical microscopy (POM), differential scanning calorimetry (DSC), and XRD results revealed that the solid-phase behavior of such two-component mixtures (acid/base = 2:1) varied significantly upon changing the proton-acceptor part from BP to OPV. Interestingly, the XRD pattern of these acid/base mixtures after annealing at their associated isotropic temperature was significantly different from that of their xogels.

**Keywords:** gels • liquid crystals • regioisomer control • self-assembly • X-ray diffraction

## Introduction

Gels are solid-like viscoelastic materials despite the presence of a major amount of solvent molecules associated with a minute quantity of the gelator (typically 0.1–10 wt %) as a minor component.<sup>[1]</sup> According to Flory, a gel could be defined as a material that has a continuous structure with macroscopic dimensions and rheologically solid-like properties.<sup>[2]</sup> Low molecular-mass organic gelators (LMOGs) form gels through multiple non-covalent forces, such as hydrogen-bonding,  $\pi$ - $\pi$ , dipole-dipole, electrostatic, van der Waals interactions, and so on.<sup>[1a]</sup> The high available surface area of the self-assembled-nanostructures (i.e., fibers, sheets, plates, rods, tubules, vesicles, and so on) formed in the gel phases is

considered to be the main reasons for physical gelation.<sup>[3]</sup> LMOGs include a wide variety of materials that are derived from sugar,<sup>[4]</sup> dendrimer,<sup>[5]</sup> oligo(*p*-phenylenevinylene),<sup>[6]</sup> cholesterol,<sup>[7]</sup> urea,<sup>[8]</sup> porphyrin,<sup>[9]</sup> amino acid,<sup>[10]</sup> and so on, which are capable of exhibiting efficient gelation in different solvents. Among them, OPV-based gelators of well-defined nanostructures have become an emerging class of gelators, especially from the last decade.<sup>[6]</sup> These molecules form gels as a result of cooperative hydrogen-bonding,  $\pi$ - $\pi$  stacking and van der Waals interactions.<sup>[6]</sup> Recently, the self-assembly of OPV-based molecules has attracted considerable attention in the design of artificial light-harvesting (LH) assemblies,<sup>[6c,e]</sup> self-assembled organic molecular wires,<sup>[11]</sup> G-quadruplex-like self-assembled organic nanoparticles,<sup>[12]</sup> molecular electronic devices,<sup>[6a]</sup> and so on. Furthermore, it has been also used to prepare various functional nanocomposites with different types of inorganic nanotubes and carbon allotropes.<sup>[13]</sup>

LMOGs comprising of a single molecular unit in the self-assembly are known as single-component gelators.<sup>[6,8,9,14]</sup> Sometimes, structurally two different components, which are non-gelators or at least one of them is a non-gelator, form efficient gels at certain molar ratios. These are known as two-component gelators.<sup>[7b]</sup> When more than two components are involved in gelation, they are known as multicom-

[a] S. Bhattacharjee, S. Datta, Prof. Dr. S. Bhattacharya  
Department of Organic Chemistry, Indian Institute of Science  
Bangalore, Karnataka 560012 (India)  
Fax: (+91) 80-23600529  
E-mail: sb@orgchem.iisc.ernet.in

[b] Prof. Dr. S. Bhattacharya  
Honorary Professor, Jawaharlal Nehru Centre for  
Advanced Scientific Research  
Bangalore, Jakkur 560064 (India)

Supporting information for this article is available on the WWW  
under <http://dx.doi.org/10.1002/chem.201302100>.

ponent gels.<sup>[15]</sup> Two-component or multi-component gelators have distinct advantages over single-component gelators because their mechanical, optical, and other properties can be conveniently tuned by changing the molar ratio of different components in the mixture.<sup>[15b,16]</sup> On the basis of molecular-level interactions among different components, the two-component gels may be classified into four categories:<sup>[10e]</sup> 1) metal-ion-coordinated gels,<sup>[17]</sup> 2) hydrogen-bonding- and halogen-bonding-induced gels,<sup>[18]</sup> 3) donor-acceptor-type gels<sup>[19]</sup> and 4) salt-type gels.<sup>[20]</sup>

Previously, we reported supramolecular hydrogelation by mixing lithocholic acid and oligomeric amines and investigated them by various physical methods to deduce the structure-property relationship with this class of soft materials.<sup>[20e]</sup> The cavities inside such gel networks could encapsulate different kinds of nanoparticles to give rise to new nanocomposites with new properties.<sup>[21]</sup> Hydrogelators derived from mixture of fatty acids and oligomeric amines may be also used to template the synthesis of Ag nanoparticles.<sup>[21]</sup> Generally, to form a salt, the  $pK_a$  value of the acid must be low compared with that of the conjugate acid of the base. Accordingly, an OPV derivative with terminal pyridyl groups could be used to verify this fact. Up to now, there are several reports in literature comprising of OPV-based single-component gelator.<sup>[6,13]</sup> Ajayaghosh et al. reported a series of single-component organogelators based on structurally divergent OPV-based systems.<sup>[6a-c,13a-b]</sup> Recently, we have also demonstrated the hydrogelation by a single-component biscationic phenylenedivinyline-based  $\pi$ -molecule.<sup>[6f]</sup> However, reports pertaining to OPV-based two-component salt-type gel are rare.<sup>[22]</sup>

Fatty acid amides of natural amino acids are also biocompatible; for example, lauric acid amide of L-alanine is an excellent phase-selective gelator, which has been shown to have potential in oil-spill remediation.<sup>[10b]</sup> *N*-Decanoyl-L-alanine (DA) is capable of exhibiting gelation in hydrocarbon solvents (i.e., *n*-hexane and *n*-heptane).<sup>[10d]</sup> Herein, we report the salt formation of DA with oligo(*p*-phenylenevinylene) functionalized with various isomeric pyridyl termini (OPV) at specific molar ratios. Various isomeric bipyridines have been chosen as a non-fluorescent analogue to compare the results with OPVs. Interestingly, the salt formation of DA modulates its aggregation properties in such a way that these acid/base mixtures are capable of forming gel in 2:1 water/ethanol system. The incumbent self-assembly phenomenon involved in the sol-to-gel transition process has been investigated by UV/Vis absorption, fluorescence, and FTIR spectroscopy. The morphological behavior and structural information of these self-assemblies have been examined by using SEM, AFM, optical profilometric experiments, and XRD techniques. Liquid-crystalline properties of the 2:1 acid/base mixtures have been explored by POM and DSC. Additionally, we have demonstrated a notable regioisomer control in gelation. Furthermore, to the best of our knowledge, this is the first time that the synthesis and characterization of two-component OPV-based salt-type hydrogel has been reported.

## Results and Discussion

**Synthesis:** Different isomeric pyridyl-appended OPV derivatives NP, NM, and NO were synthesized by using the Horner–Wadsworth–Emmons reaction (Figure 1 a). Each of the isomeric pyridine aldehydes was treated with the corresponding 1,4-di-*n*-alkoxy-2,5-biphosphonate in the presence of *t*BuOK under an Ar atmosphere (the Supporting Information). The residue obtained after the work up was leached with *n*-hexane several times to furnish the pure product (the Supporting Information). DA was synthesized according to a previously reported procedure.<sup>[10d]</sup> The final products were characterized by using <sup>1</sup>H/<sup>13</sup>C NMR spectroscopy, ESI-MS, FTIR, and elemental analysis (the Supporting Information, Figure S1–S3).

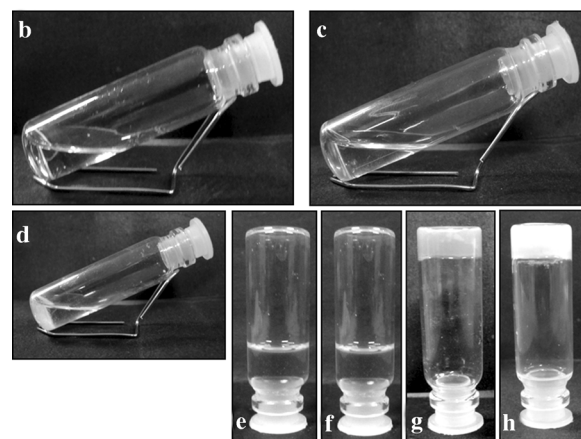
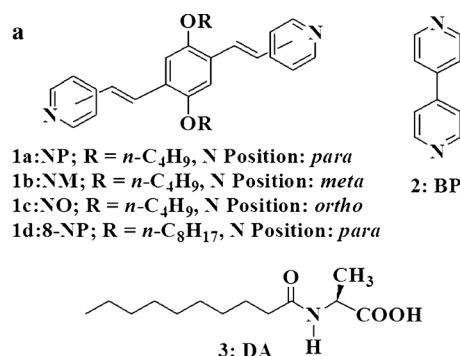


Figure 1. a) Molecular structures of the different OPVs, BP, and DA used in the present study. Photographs of solutions of b) BP and c) DA; precipitate of d) NP; e) sol of NO-DA (1:2), and f) NM-DA (1:2); typical gels of g) NP-DA (1:2) and h) BP-DA (1:2) in 2:1 water/ethanol mixture; [NP], [NM], [NO] = 4 mM, [BP] = 20 mM in each case, [DA] = 8 mM in the case of c), e)–g) and 40 mM in case of h).

**Gelation studies:** The gelation ability of *N*-decanoyl-L-alanine (DA) was checked in aqueous/ethanol (2:1) mixture in presence of various isomeric bipyridine and OPV derivatives. Each of these individual components was soluble in ethanol and gave a transparent, clear solution that never formed gel, even upon prolonged ageing. However, they were insoluble in water. Interestingly, we found that mixing of BP with two equivalents of DA in 2:1 water/ethanol mix-

ture (v/v) followed by heating at 70–75 °C gave a transparent solution, which upon subsequent cooling and sonication led to the formation of a white colored, thermoreversible, opaque gel (minimum gelator concentration [mgc] = 16.4 mM = [BP]) (Figure 1 h). It is important to note that the mixture of 2,2'-bipyridine or 3,3'-bipyridine and DA did not lead to gelation under the same conditions. This observation prompted us to synthesize OPV derivatives functionalized with various isomeric pyridyl termini (NP, NM, NO) to obtain salt-type OPV-based gels. Among them, notably only mixture of NP and DA (1:2) was able to form an orange-colored, fluorescent, thermoreversible, opaque gel in 2:1 water/ethanol (v/v) ([mgc] = 3.31 mM = [NP]) (Figure 1 g), whereas other members did not lead to gelation with DA in that solvent system. Interestingly, a 1:2 mixture of NP and DA formed a gel at much lower mgc compared with that of the BP-DA gel. Accordingly, 1 unit of NP-DA (1:2) system can hold almost 8000 water molecules and 1300 ethanol molecules inside the three-dimensional gel network. The chain length of the OPV backbone is also important in determining the effect on gelation. Accordingly a control compound, **8-NP** was synthesized (Figure 1 a). Interestingly, **8-NP** formed a precipitate with DA in a 2:1 water/ethanol mixture. This result clearly elucidates that a hydrophilic/hydrophobic balance is crucial for the gelation of this system.

Salt formation of each of NP, NM, and NO was also checked in presence of different fatty acids of variable chain lengths as well as aromatic acids, such as benzoic acid. Among them, only NP resulted in the salt formation with these acids, whereas NM and NO failed. Interestingly, the salt of NP with fatty acids of variable chain lengths (no. of carbon atoms ( $n$ ) = 8, 10, 12, 14, 16) led to the formation of gelatinous precipitates in the 2:1 water/ethanol mixture. This signifies that the hydrogen bonding through amide units of DA is very important and plays a crucial role in the aggregation as well as hydrogelation. Benzoic acid was chosen as the simplest among the aromatic acids, which also resulted in the formation of precipitate with NP in that solvent system, because of the lack of both flexible aliphatic hydrocarbon chain and hydrogen-bonding motif. Thus apart from the acidity, the lipophilic/hydrophilic balance as well as the flexibility and hydrogen bonding all contribute to the gelation.

**The role of basicity in selective gelation:** The gelation properties of the OPV derivatives in presence of DA was found to depend on the basicity of the "N" atom of the pyridyl ring. We thought that it is important to determine the  $pK_a$  values of these compounds to find out the reason of selective gelation by NP. Accordingly, we obtained the  $pK_a$  values of these pyridine derivatives experimentally.

Since the protonated and non-protonated forms of these OPV derivatives absorb differently, UV/Vis spectroscopy was used as an efficient tool to determine their  $pK_a$  values.<sup>[23]</sup> We recorded the UV/Vis absorption spectra of these compounds in 0.1 M sodium formate/formic acid and phosphate/citrate buffer solutions of various pH values and

the  $pK_a$  value of each of these series of compounds was obtained from the plots of the absorbance versus pH. The experimentally determined  $pK_a$  values of NP in 0.1 M sodium formate/formic acid and phosphate/citrate buffer solutions are 3.77 and 3.72, respectively (Figures S4 and S5, the Supporting Information). So, the average  $pK_a$  value of NP is  $3.75 \pm 0.04$ . Similarly, the experimentally determined  $pK_a$  value of NM is  $3 \pm 0.11$  (Figures S6 and S7, the Supporting Information), whereas NO remains unprotonated even at pH 2.8. This is clearly evident from the broad absorption spectra of NO in sodium formate/formic acid buffer solution (Figure S8, the Supporting Information). According to the experimentally determined  $pK_a$  values, the order of basicity of these OPVs is  $NP > NM > NO$ .

Proton transfer during an acid/base reaction depends on the  $\Delta pK_a$  value ( $pK_a$  of the conjugate acid of pyridine base –  $pK_a$  of the carboxylic acid).<sup>[24]</sup> When  $\Delta pK_a < 0$ , it results in a neutral O–H...N–H bond. On the other hand,  $0 < \Delta pK_a < 3$  gave an intermediate O–H...N/N<sup>+</sup>–H...O<sup>–</sup> hydrogen-bond character. However,  $\Delta pK_a > 3$  results in complete proton transfer to induce an ionic interaction N<sup>+</sup>–H...O<sup>–</sup>. Therefore, NP with relatively higher basicity should be able to form a salt with DA with an intermediate O–H...N/N<sup>+</sup>–H...O<sup>–</sup> hydrogen-bond character, which accounts for the reason of selective gel formation by NP. Whereas, NM and NO, being relatively less basic compared with NP, most likely fail to form a salt with DA. Furthermore, in case of NO, the pyridyl "N" atom is probably buried under the  $\pi$ -cloud of the OPV backbone. This results in a crowding effect, which may be an alternative reason of the inability of NO towards salt formation. It is important to note that  $pK_a$  was measured in pure buffered aqueous media. However, the gelation was performed in 2:1 water/ethanol mixture, and there will be changes in the  $pK_a$  values in ethanolic aqueous media. Moreover, it is known that  $pK_a$  values of different pyridine derivatives show changes at interfaces.<sup>[25]</sup> Thus, the  $pK_a$  of various isomeric OPV derivatives may also change upon self-assembly. However, the extent of change in  $pK_a$  would be probably similar for the three isomers. So, the trend in these values may explain the selective salt formation and gel formation phenomena as observed here.

**Computational studies:** The main factor that governs the selective gel formation is the protonation of NP by DA, and thereby self-aggregation of NP-DA (1:2) using several weak non-covalent interactions leads to robust gel formation. To obtain a reasonable explanation of these observations, each of these molecules in the form of the HCl salt were optimized by using the B3LYP G/6-31G\* level of theory (Figure 2). HCl was chosen as a proton source to mimic the real situation. For these purposes, the two most relevant conformations were considered; one in which the attached N atom of the end pyridyl ring was placed facing towards the vinylic bond and one in which the attached N atom was placed away from the vinylic bond (in case of NM-HCl and NO-HCl; Figure 2 b and c). In striking contrast, only one conformation was possible for NP-HCl, in which the at-

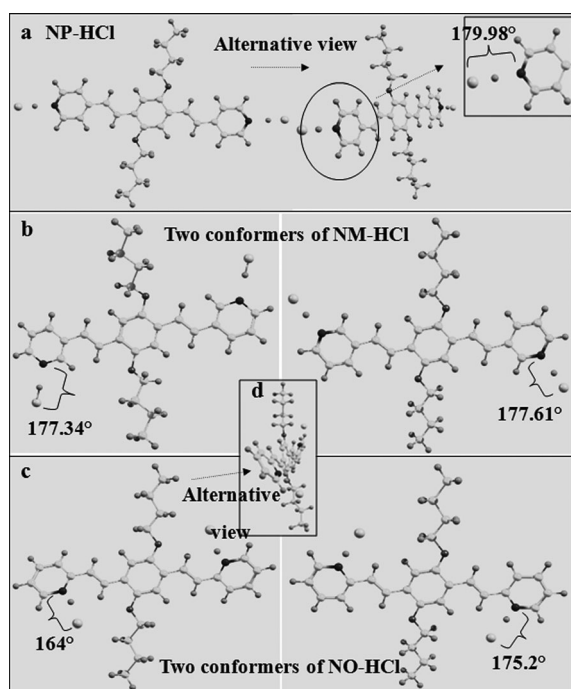


Figure 2. Energy-minimized structures of a) NP-HCl, b) NM-HCl, and c) NO-HCl; d) Distortion of  $\pi$ -aromatic backbone of NO-HCl.

tached N atom was placed in the *para* position to the end pyridyl ring. Energy minimization of NP in the form of the HCl salt shows almost negligible distortions in the planar  $\pi$ -aromatic backbone (Figure 2a). Moreover, the N–H–Cl angle in the energy minimized structure was linear ( $179.98^\circ$ ), indicating that HCl forms a salt with NP without any significant distortion of the OPV backbone.

On the other hand, energy minimization of NM (for the two conformations) in the form of HCl salt gave the lowest energy as  $E = -2267.726$  and  $-2267.808$  a.u., respectively, both of the values are a little bit larger than the lowest energy of the NP-HCl salt ( $E = -2267.810$  a.u.). Additionally, the N–H–Cl angle in the energy-minimized structure of NM-HCl was distorted to  $177.335$  and  $177.611^\circ$ , respectively, in the most probable two conformations, indicating that protonation of NM could be also achieved, although with additional difficulty compared to that of NP.

In case of NO-HCl in which the N is away from the vinylic bond, the N–H–Cl angle was found to be  $175.2^\circ$ . Whereas, in NO-HCl in which the N is buried and/or close to the vinylic bond, the N–H–Cl angle experiences the greatest degree of distortion of about  $164^\circ$  ( $\Delta$ distortion ca.  $16^\circ$ ). Moreover, the  $\pi$ -aromatic core experiences a high distortion from the planarity to accommodate HCl, and to minimize the energy of NO-HCl salt, meaning that HCl forms a salt with NO with great difficulty. It is important to note the distortion of aromatic core and the N–H–C angle was greatest in case of NO-HCl, followed by NM-HCl. Whereas NP-HCl experiences the least distortion in both cases. The results obtained from computational studies are in accord with the basicity trend of the OPVs.

To investigate the actual situation, computational studies were further performed on NP-DA, NM-DA, and NO-DA systems (the Supporting Information, Figure S9). NP experiences negligible distortion from planarity as well as N–H–O angle ( $179.97^\circ$ ) in the case of NP-DA system. However, the distortion of  $\pi$ -aromatic backbone of NM in case of NM-DA (for the two conformers) and the deviation of the N–H–O angle ( $179.31$  and  $179.36^\circ$ , respectively) from linearity was moderate. In stark contrast, NO-DA (for the two conformers) experiences a maximum distortion of  $\pi$ -aromatic backbone and deviation of the N–H–O angle ( $177.71$  and  $178.50^\circ$ , respectively) from linearity with the lowest energy of  $E = -2928.054$  and  $-2928.044$  a.u., respectively, both of which are considerably larger than the lowest energy of NM-DA system ( $E = -2928.066$  and  $-2928.065$  a.u., respectively, for the two conformers). Thus, the computational studies provide an explanation of the selectivity in terms of gel formation.

**FTIR Spectroscopy:** FTIR spectroscopy provides a useful way to investigate the primary interactions involved in the gelation of two-component systems, for example, acid and base. DA in its solid state has a –OH stretching frequency of the –COOH group at  $3348\text{ cm}^{-1}$ . However, when mixed with NP at a 1:2 molar ratio, this band shifted to a lower frequency of  $3300\text{ cm}^{-1}$  and a shoulder appeared at  $3340\text{ cm}^{-1}$  indicating the formation of a salt (the Supporting Information, Figure S10). Similarly, the –OH stretching of DA shifted to  $3290\text{ cm}^{-1}$  in 1:2 stoichiometric mixture of BP and DA.

The appearance of the amide I band at  $1644\text{ cm}^{-1}$  for the BP-DA xerogel and at  $1645\text{ cm}^{-1}$  for NP-DA xerogel indicates the presence of strong intermolecular hydrogen-bonding between –CONH groups (the Supporting Information, Figure S10).<sup>[26a]</sup> The FTIR spectrum of DA showed a broad C=O absorption associated with the carboxylic acid group in the range of  $1726\text{--}1707\text{ cm}^{-1}$ , which was almost silent in case of NP-DA (1:2) and BP-DA (1:2) systems. This observation clearly suggests the transfer of the –COOH proton to the basic pyridine N-atom of NP or BP.<sup>[26b]</sup> In addition, the appearance of new peaks at  $1615$  and  $1604\text{ cm}^{-1}$  for NP-DA and BP-DA xerogels, respectively, in the low-frequency region further proves the dissociation of the carboxylic acid and the formation of anionic –COO<sup>–</sup> species.<sup>[26a]</sup>

**SEM, AFM, and optical profilometry experiments:** To discern the microstructures present in the three-dimensional (3D) networks of the gelators, we examined these gel samples by SEM and AFM. Representative SEM images of the BP-DA mixtures showed fiber-like nanostructures at four different molar ratios. The fibers are of very high aspect ratios with several hundreds of micrometers length and diameters ranging from about  $0.7$  to  $7.7\text{ }\mu\text{m}$  (Figure 3a–d). On the other hand, the SEM image of NP-DA (1:0.5 to 1:2), exhibited the presence of rectangular plate-like morphologies (Figure 3e–h). Generally, the fibers or sheet-like structures are found in most of the gels reported. Hence, the present

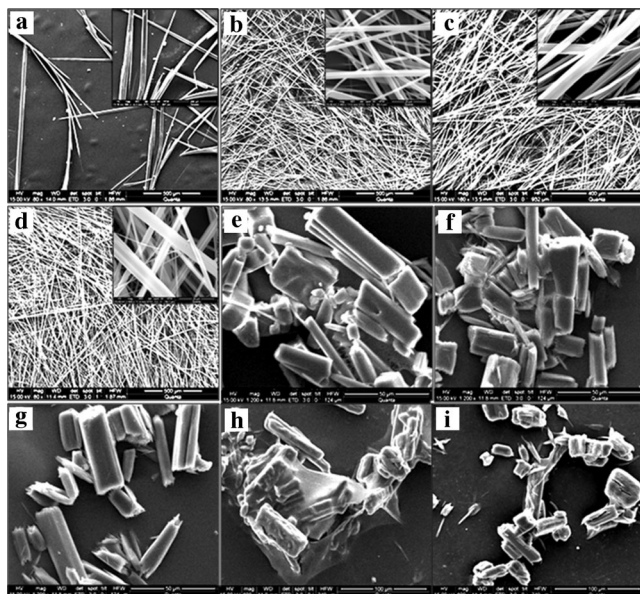


Figure 3. SEM images of BP-DA at different molar ratios of a) 1:0.5, b) 1:1, c) 1:1.5, and d) 1:2, respectively; [BP]=7.18 mm in each case, [DA]=3.59, 7.18, 10.77, and 14.37 mm, respectively. SEM images of NP-DA at different molar ratios of e) 1:0.5, f) 1:1, g) 1:1.5, h) 1:2, and i) 1:3, respectively; [NP]=5.8 mm in each case, [DA]=2.9, 5.8, 8.7, 11.7, and 17.5 mm, respectively.

work is a rare example in which rectangular gel particles have been observed in the xerogel. Sada and co-workers also reported the formation of uniform cubic gel particles with well-defined edges and square faces using internal cross-linking of the CD-MOF crystals followed by loss of coordinating metal ions.<sup>[27]</sup> However, with increasing the stoichiometry of DA, the rectangular plates gradually abolished and self-assembled clusters were formed (Figure 3 i).

The superstructures created in the gel network of 1:2 mixture of BP-DA were also observed under AFM. AFM images of the BP-DA system at different molar ratios also showed fibrous networks, which is in accord with the SEM finding (Figure 4 a–d). To investigate the rectangular plate-like morphology of the NP-DA in detail, an optical profilometric experiment was carried out for NP-DA at different molar ratios (Figure 4 e–i). A rectangular plate-like morphology was observed for NP-DA up to a stoichiometric ratio of 1:1.5. However, the plate-like morphology was almost abolished and some cluster-type microscopic particles were observed at amine/acid ratios of 1:2 and 1:3. Importantly, the plates were of different heights and in some cases the plates conserved their smoothness over large areas. Since the height of these microplates was more than 5  $\mu\text{m}$ , we could not visualize them adequately by AFM. It is well-known that molecular chirality can induce supramolecular chirality efficiently in the self-assembled supramolecular fibers.<sup>[6b,22a,28]</sup> For example, Schenning and Meijer et al. have described the fabrication of self-assembled 1D stacks by a chiral supramolecular auxiliary approach.<sup>[28]</sup> However, in the present case we have not observed any chiral amplification to the supramolecular level.

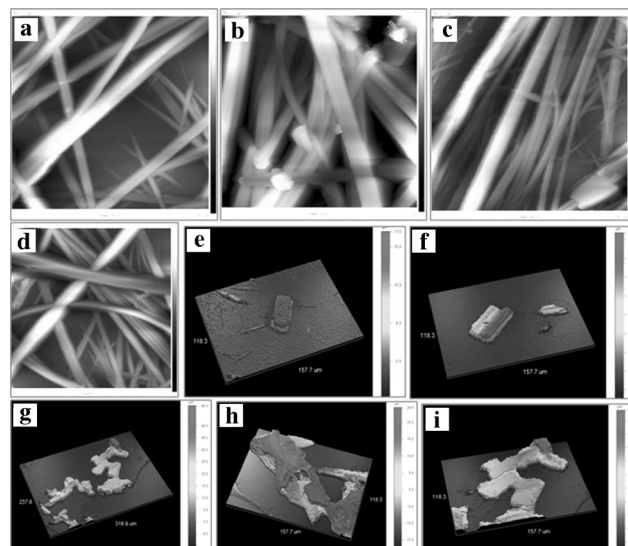


Figure 4. AFM images of BP-DA at molar ratios of a) 1:0.5, b) 1:1, c) 1:1.5, and d) 1:2, respectively; [BP]=7.18 mm in each case; [DA]=3.6, 7.2, 10.8, and 14.4 mm, respectively. Optical profilometric images of NP-DA at molar ratios of e) 1:0.5, f) 1:1, g) 1:1.5, h) 1:2, and i) 1:3, respectively; [NP]=5.8 mm in each case, [DA]=2.9, 5.8, 8.7, 11.7, and 17.5 mm, respectively.

**UV/Vis and fluorescence spectroscopy:** Thermoreversibility and molecular interactions involved in the gel-to-sol transition process were followed by temperature-dependent UV/Vis absorption spectroscopy. These systems show broad absorption spectra at their associated minimum gelator concentrations and the sigmoidal nature of the gel melting plot was an indication of an isodesmic mechanism during self-assembly (the Supporting Information, Figures S11 and S12).<sup>[14b]</sup> Since aggregation was still present at low concentrations, we recorded their UV/Vis spectra in dilute solutions.<sup>[14b]</sup> Two absorption maxima ( $\lambda_{\text{max}}$ ) at 352 and 439 nm, respectively, were observed for the NP-DA (1:2) system in 2:1 water/ethanol mixture at 20 °C and shifted to 341 and 423 nm at 60 °C, indicating a gradual change in the aggregated absorption to monomeric absorption (Figure 5 a). This phenomenon clearly reveals a J-type aggregation of the OPV-based gelator.<sup>[9b,10g]</sup> The intensity of absorption increases with concomitant increase of temperature. This may be explained on the basis of heat-induced "destacking" of the  $\pi$ -aromatic backbone of the NP-DA (1:2) system and subsequent generation of monomeric unit, which has higher molar absorptivity ( $\epsilon$ ) compared with the self-assembled molecular aggregates. The transition temperature (ca. 42 °C) associated with the melting of the aggregates was calculated from the plot of Abs.<sub>439</sub> versus temperature (the Supporting Information, Figure S13 a). The sigmoidal nature of the plot indicates that an isodesmic mechanism is probably followed during the aggregation process.<sup>[29]</sup> In contrast, the BP-DA (1:2) system exhibited only one absorption maximum at 239 nm at 20 °C and did not show any significant shift in the absorption spectra upon increasing the temperature (the Supporting Information, Figure S14).

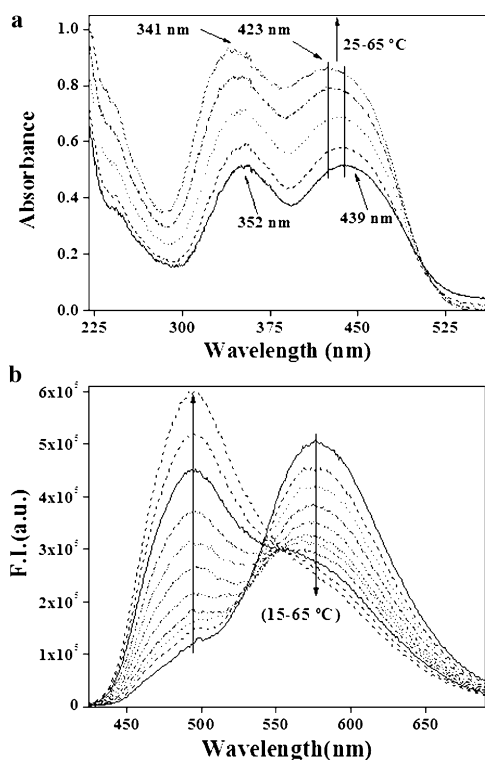


Figure 5. Temperature-dependent changes in the a) UV/Vis absorption ([NP]=0.29 mM; [DA]=0.58 mM) at 25, 35, 45, 55, and 65 °C and b) fluorescence spectra of NP-DA (1:2) in water/ethanol (2:1) mixture ([NP]=0.23 mM; [DA]=0.46 mM) at 15, 20, 25, 30, 35, 40, 45, 50, 55, 60, and 65 °C.

A salt-type interaction-mediated selective gelation of NP with DA has been further explored by following stoichiometry-dependent absorption spectroscopy in 2:1 water/ethanol. Figure S15a (the Supporting Information) shows that two peaks in the UV/Vis spectra appear at 334 and 405 nm, respectively, at a 1:0.5 stoichiometric ratio of NP-DA. It shifted to 350 and 433 nm, respectively, in the 1:2 mixture of NP-DA, which was accompanied by a significant increase in the intensity of absorption. This result is further supported by the change in visible color of the solution from nearly colorless to deep-yellow on increasing the molar ratio of DA (the Supporting Information, Figure S15b). Schenning and Meijer et al. have also reported similar large color shifts as a result of formation of hydrogen-bonded ion pair.<sup>[28]</sup> However, the UV/Vis peak at 380 nm in 1:0.5 mixture of NM-DA exhibited a redshift of around 5 nm followed by a little increase in the absorption intensity on gradual addition of DA starting from 0.5 to 2 equiv (the Supporting Information, Figure S16). Interestingly, no significant shift and change in the intensity were observed in case of NO with increasing proportion of DA (the Supporting Information, Figure S17). This phenomenon clearly elucidates that NP is readily able to form a salt with DA leading to gelation. In contrast, NM and NO did not result any gel formation because of their inability to induce salt formation with DA.

The J-type aggregation mode of the OPV-based gelator was further investigated by recording changes in the temper-

ature-dependent fluorescence spectra. The fluorescence spectra of a 1:2 mixture of NP and DA in 2:1 water/ethanol (v/v) showed one emission maximum at 576 nm associated with the aggregated species and a shoulder at 494 nm at 15 °C (Figure 5b). However, the emission intensity at 576 nm gradually diminished, which was followed by the appearance of a blueshifted hyperchromic peak at 494 nm (isotropic emission) when increasing the temperature from 15 to 65 °C. This indicates an apparent breakdown of the supramolecular aggregates on heating. Conversely, the redshift of the emission maximum as a result of self-aggregation clearly ascribes to the presence of J-type aggregation mode of this gelator system. The melting temperature (ca. 42 °C) of the aggregates is obtained from the plot of F.I.<sub>576</sub> (fluorescence intensity at  $\lambda = 576$  nm) versus temperature and the result is in good agreement with the findings obtained on the basis of the UV/Vis absorption spectroscopy (the Supporting Information, Figure S13b).

#### Differential scanning calorimetry (DSC) and polarized optical microscopy (POM):

Hydrogen bonding and salt formation have been used previously to congregate a carboxylic acid derivative with compounds having a terminal-pyridyl group to produce calamitic or linear rod-shaped structural organizations, which in turn exhibit a mesogenic behavior.<sup>[30]</sup> Keeping this in mind, DA was mixed with either BP or NP at 1:2 molar ratio in THF. After evaporation of the solvent, the solid residue was investigated using POM, DSC, and XRD techniques. In the first heating cycle of the DSC experiment, the solid sample was heated (25–150 °C) to melting to remove the anisotropic history of the sample. Then the resulting melt was cooled down at a rate of 5 °C min<sup>-1</sup>. After the melt reached room temperature, new heating and cooling cycles were performed under the same conditions as before. Under these conditions, a 1:2 mixture of NP-DA showed an endothermic transition at 104.5 °C (Figure 6a). Interestingly, in the cooling cycle, it exhibited double exothermic transitions at 121 and 79.5 °C, respectively (Figure 6a). A smaller peak appeared at higher temperature and a larger exothermic transition appeared at lower temperature during the cooling cycle. However, the DSC thermograms of BP-DA (1:2) showed only a single and sharp peak at 103.5 °C during the heating and at 72.5 °C in the cooling cycle (Figure 6a).

Thermotropic properties of these acid/base mixtures were further probed by using temperature-dependent polarized optical microscopy. The samples were first heated to obtain an isotropic melt (Figure 6b) and then slowly cooled down to room temperature at the same rate of the DSC experiment (5 °C min<sup>-1</sup>). Thermotropic transitions were observed during cooling of the isotropic melt and different birefringent patterns appeared upon changing the temperature. For the 1:2 stoichiometric NP-DA mixture, a straw-like texture started appearing at about 120 °C, which was associated with a small exothermic transition in the DSC profile (Figure 6c).<sup>[31b]</sup> Interestingly, fan-shaped focal conic textures corresponding to the smectic-A (SmA) phase appeared at

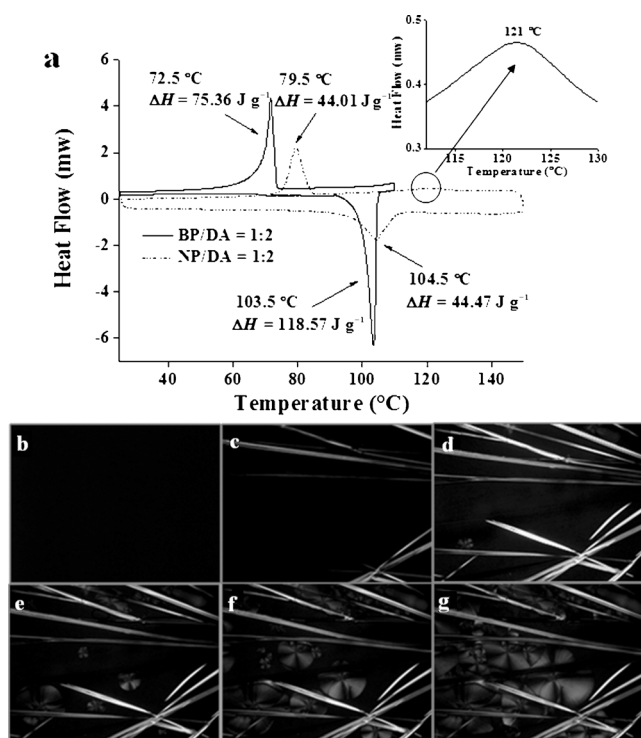


Figure 6. a) Solid-phase DSC profile of NP-DA (1:2) and BP-DA (1:2), respectively; inset shows magnification of exothermic scan of NP-DA for clarity. POM images of NP-DA (1:2) were captured at b) 130 (isotropic), c) 120, d) 80, e) 75, f) 65, and g) 60 °C.

about 80 °C under a polarizing microscope, which gave a sharp peak in the DSC experiment (Figure 6 d–g).<sup>[31c]</sup> However, a fingerprint texture was found at about 72 °C during the cooling of the isotropic melt of the 1:2 mixture of BP and DA (the Supporting Information, Figure S18).<sup>[31a]</sup> The associated transition in DSC appeared as a sharp exothermic peak at 72.5 °C with a large enthalpy change of 75.36 J g<sup>-1</sup>. However, a phase transition from the LC phase to a crystalline phase or glass transition was not observed in DSC, probably due to the slow transition between the respective phases.<sup>[32]</sup>

**Rheology experiment:** Gels are viscoelastic solid-like materials, and the viscoelastic properties of gels are best characterized by rheological studies.<sup>[6d,f]</sup> Therefore, oscillatory frequency-sweep and amplitude-sweep experiments were performed to find out the elastic and loss moduli ( $G'$  and  $G''$ ). The elastic modulus  $G'$  represents the solid-like character, that is, the ability of the material to defy deformation, whereas the loss modulus  $G''$  reflects the liquid-like behavior, that is, the tendency of the material to flow. Generally, gels exhibit a higher magnitude of the  $G'$  value than the  $G''$  value, demonstrating viscoelastic character. In an oscillatory amplitude-sweep experiment, the switchover point of  $G'$  and  $G''$  is termed as yield stress ( $\sigma_y$ ), in which a transition of the elastic solid-like character to a viscous liquid-like character occurs.

The oscillatory frequency-sweep experiments were carried out for both BP-DA (1:2) and NP-DA (1:2) gels. The frequency-sweep experiment revealed that the storage modulus  $G'$ , was always greater than the respective loss modulus  $G''$  under an applied stress of 1 Pa in the frequency range of 0.1–10 Hz, thereby indicating the viscoelastic nature of the gel over the entire angular frequency range (Figure 7 a).

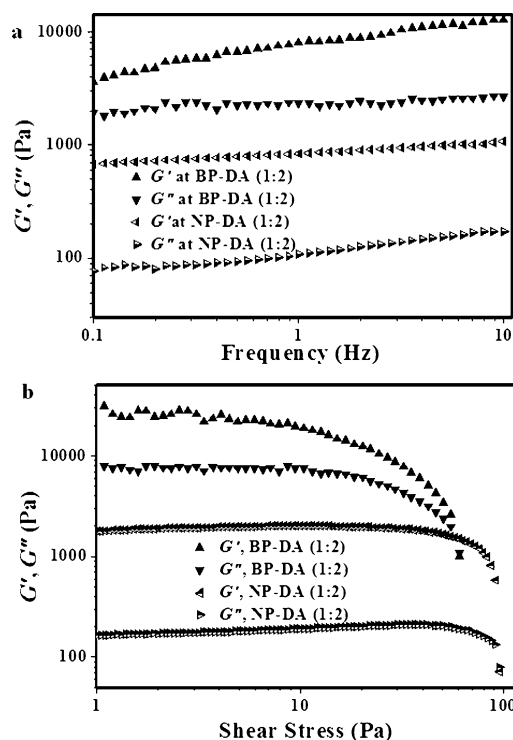


Figure 7. a) Frequency- and b) amplitude-sweep rheology data of NP-DA (1:2) and BP-DA (1:2) in a 2:1 water/ethanol mixture; [BP] and [NP] = 18.7 mM, [DA] = 37.4 mM.

To compare the mechanical properties of these two-component gels, an oscillatory amplitude-sweep experiment was performed. Each gel showed its own characteristic yield stress ( $\sigma_y$ ) according to its viscoelasticity to an oscillating stress at the concentration of 18.7 mM. When these salt-type gels succumbed to an applied stress, the gel composed of BP-DA (1:2) started to flow at a shear stress of about 85 Pa. However, the NP-DA (1:2) gel began to lose its solid-like behavior at a critical stress of about 95 Pa (Figure 7b). Therefore, the gel of NP-DA is more resistant to flow under an applied mechanical force than that of the BP-DA gel. Moreover, an oscillatory amplitude-sweep experiment was also performed for NP-DA (1:2) gel at different concentrations in 2:1 water/ethanol (v/v) mixture (the Supporting Information, Figure S19). The yield stress progressively increased with increasing gelator concentration. This observation clearly demonstrated the gradual increase in the viscoelasticity of the NP-DA gel with increasing concentrations.

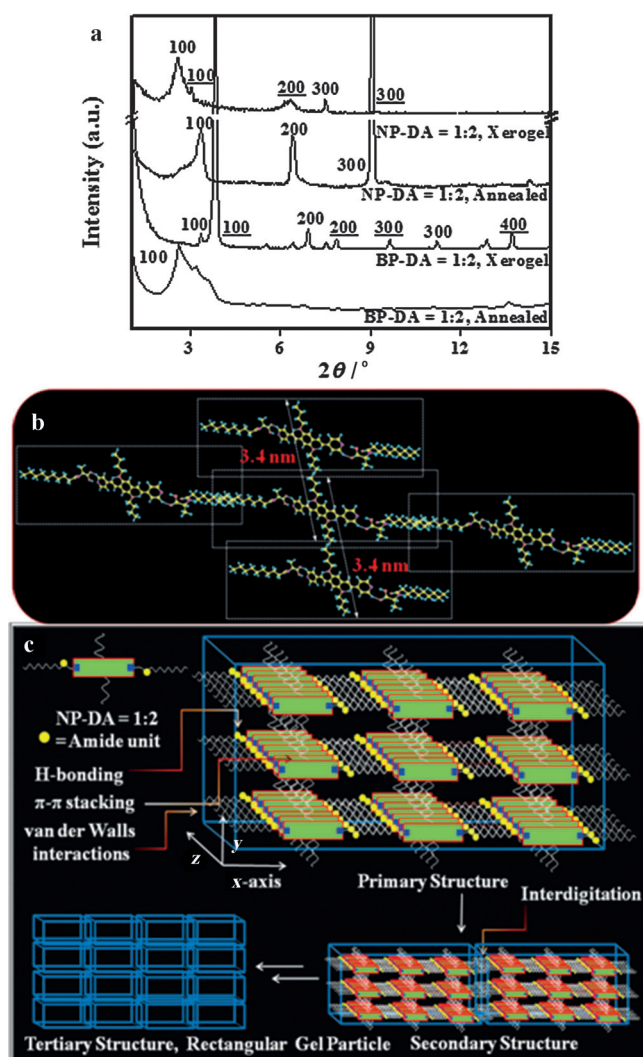


Figure 8. a) XRD plots of xerogels of NP-DA (1:2), BP-DA (1:2) from a 2:1 water/ethanol mixture and annealed solid of NP-DA (1:2), BP-DA (1:2). b) Proposed molecular packing of propagation of the aggregates of NP-DA (1:2). c) A proposed model depicting the formation of rectangular gel particles by the NP-DA (1:2) system.

**X-ray diffraction and molecular modeling:** X-ray diffraction was performed to unveil the mechanism of packing of the supramolecular organizations in the xerogels. Figure 8a shows the diffraction pattern of the xerogel obtained from a 1:2 mixture of NP and DA in 2:1 water/ethanol mixture. It shows two sets of Bragg reflections. The corresponding  $d$ -values of these two sets of peak are  $d_1=3.4$  nm,  $d_2=1.14$  nm (1/3) and  $d'_1=2.8$  nm,  $d'_2=1.44$  nm (1/2),  $d'_3=0.93$  nm (1/3), respectively. These results clearly indicate the presence of two sets of lamellar structures in the gel network with the interlayer spacings of 3.4 and 2.8 nm, respectively. Interestingly, the longest interlayer spacing (3.4 nm) is equal to the double of its molecular length (1.7 nm) along the direction of  $-\text{OC}_4\text{H}_9$  backbone as calculated by an optimization of geometry of the single molecule using B3LYP/6-31G\* level of theory (Figure 8b).

X-ray diffraction (XRD) plots of the xerogel of 1:2 mixtures of BP and DA show the presence of two sets of lamellar structures. The corresponding  $d$ -spacings of these two sets are  $d_1=2.62$ ,  $d_2=1.28$  (1/2),  $d_3=0.9$  (1/3),  $d_4=0.65$  nm (1/4) and  $d'_1=2.3$ ,  $d'_2=1.12$  (1/2),  $d'_3=0.78$  nm (1/3), respectively. This indicates the presence of a lamellar arrangement in the three-dimensional (3D) gel network with interlayer spacing of 2.62 and 2.3 nm, respectively. However, only a broad peak at 1.3 nm has been observed in the XRD plot of the annealed mixture of BP-DA (1:2). All of these results clearly demonstrate the different modes of aggregation in the gel phase and solid state. Moreover, the XRD pattern of these two-component systems are completely different from that of the individual component (the Supporting Information, Figure S21).

Furthermore, the structural changes associated with the birefringence textures were monitored by temperature-dependent XRD. The relevant diffractograms of NP-DA at variable temperatures were recorded and shown in Figure S22 (the Supporting Information). Interestingly the XRD patterns of the NP-DA (1:2) system under these conditions showed significant differences from that of the xerogel. At 130°C, no diffraction was observed, indicating an isotropic liquid state of NP-DA. However, gradual cooling to 115°C and subsequent data collection manifested only a few diffraction peaks that correspond to the straw-like textures. Moreover, appearance of only few peaks also indicates "loose" molecular packing (low enthalpic transition) that, in turn, presumably causes very weak exothermic transition in the DSC experiment at around 121°C.<sup>[32]</sup> On further cooling, the sample at 75°C showed four major reflections at 2.6, 1.3, 0.95, and 0.67 nm, respectively, along with some small peaks associated with the fan-shaped focal conic liquid-crystalline phase. Interestingly, the solid material at 25°C, exhibited only three reflections. The corresponding  $d$ -values are  $d_1=2.6$  nm,  $d_2=1.3$  nm (1:2), and  $d_3=0.86$  nm (1:3) indicating a lamellar-type arrangement. Furthermore, the longest  $d$ -spacing (2.6 nm) is less than the double of its molecular length (1.7 nm) as calculated from an optimization of geometry of the single molecule using B3LYP/6-31G\*. This analysis indicates that the  $-\text{OC}_4\text{H}_9$  chains interdigitate with each other to introduce effective van der Waals interactions among the  $-\text{OC}_4\text{H}_9$  chains. Interestingly, the diffraction pattern at 25°C exactly matched with the diffraction pattern of the annealed sample of 1:2 mixture of NP and DA. It is important to note that the diffraction pattern of the annealed sample of 1:2 mixture of NP and DA shows significant differences from that of the xerogel.

As stated above, a rectangular gel particle was observed instead of a fiber formation. It is possible that the gelation observed here involves a frustrated crystallization process.<sup>[1a,33]</sup> In fact, there are several reports in which the crystallization of the gelator molecule was achieved inside the 3D-gel network.<sup>[18g,33]</sup> Although in such cases, the gelator molecules have substantial crystalline character (i.e., absence of long-chains, which usually decreases the crystallinity of a compound). Indeed, gelation occurs when the pro-

density of crystallization (i.e., the conversion of the solid component into crystal from the respective solution) is mitigated.<sup>[1a]</sup> In the present case, NP is crystalline in nature due to the presence of short  $-OC_4H_9$  chains and DA is amorphous because it has a long *n*-decanoyl chain in its structure. As a result, the combination of NP and DA in 1:2 molar ratios by simple acid/base interactions led to a semi-crystalline composite, which, in turn, presumably yielded micro-crystalline rectangular gel particles. Moreover, the formation of fibrous (linear) aggregates is governed by the direction and strength of the binding forces among the aggregates of the gelators.<sup>[1a]</sup> In the present case, the interactions among the aggregates of NP–DA (1:2) are probably not strong enough to form such directional (fibrous) aggregates with high aspect ratios, thus resulting in the formation of the rectangular gel particle. Furthermore, when NP and DA was mixed in 1:3 molar ratio, the overall crystallinity of these composites was found to be even less compared with that of the NP–DA (1:2) system. This resulted in the formation of self-assembled clusters instead of forming rectangular gel particle. Based on this rationale, a model has been proposed for the formation of such rectangular gel particles (Figure 8c).

## Conclusion

We have demonstrated here the selective two-component gelation by a 1:2 mixture of NP–DA system over the NM–DA or NO–DA system in 2:1 water/ethanol (v/v). The basicity of the "N" atom of the pyridyl ring was found to be the most important factor in determining the selectivity of gel formation. Selective gelation of NP–DA over NM–DA and NO–DA was rationalized by using computational studies. The acid/base interaction involved in the sol-to-gel transition was confirmed unambiguously by FTIR and UV/Vis spectroscopy. Temperature-dependent UV/Vis and fluorescence spectroscopy revealed the presence of *J*-type aggregation modes with the NP–DA gelator system. Unlike the BP–DA gelator, which showed the presence of fibrous morphology, the NP–DA gel manifested the presence of rectangular plate-like gel particles under SEM. The optical profilometric experiment also supported the SEM results. The existence of the two sets of lamellar structures in the three-dimensional gel network was confirmed by XRD experiments for both the systems. In addition to the gelation phenomena, the liquid-crystalline behavior of these two-component mixtures was investigated by POM and DSC experiments. During cooling of the isotropic melt under a polarized optical microscope, a fingerprint-like lamellar structure was observed for the mixture of BP and DA (1:2). However, a double-phase transition was observed for the NP–DA (1:2) system. In a nutshell, we have demonstrated not only the two-component, salt-type hydrogelation of an OPV derivative for the first time, by supramolecular polymerization with rare gel morphology, but also evidenced excellent liquid crystallinity from these two-component mixtures.

## Acknowledgements

This work was supported by J. C. Bose fellowship of DST to S.B. S.B. and S.D. thank CSIR for senior research fellowship.

- [1] a) P. Terech, R. G. Weiss, *Chem. Rev.* **1997**, *97*, 3133–3159; b) D. J. Abdallah, R. G. Weiss, *Adv. Mater.* **2000**, *12*, 1237–1247; c) M. de Loos, B. L. Feringa, J. H. van Esch, *Eur. J. Org. Chem.* **2005**, 3615–3631; d) A. R. Hirst, B. Escuder, J. F. Miravet, D. K. Smith, *Angew. Chem.* **2008**, *120*, 8122–8139; *Angew. Chem. Int. Ed.* **2008**, *47*, 8002–8018; e) G. O. Lloyd, J. W. Steed, *Nat. Chem.* **2009**, *1*, 437–442.
- [2] P. J. Flory, *Faraday Discuss. Chem. Soc.* **1974**, *57*, 7–18.
- [3] L. A. Estroff, A. D. Hamilton, *Chem. Rev.* **2004**, *104*, 1201–1217.
- [4] a) S. Bhattacharya, S. N. G. Acharya, *Chem. Mater.* **1999**, *11*, 3504–3511; b) O. Gronwald, E. Snip, S. Shinkai, *Curr. Opin. Colloid Interface Sci.* **2002**, *7*, 148–156; c) A. Srivastava, S. Ghorai, A. Bhattacharjya, S. Bhattacharya, *J. Org. Chem.* **2005**, *70*, 6574–6582; d) G. John, G. Zhu, G. Li, J. S. Dordick, *Angew. Chem.* **2006**, *118*, 4890–4893; *Angew. Chem. Int. Ed.* **2006**, *45*, 4772–4775; e) J. Cui, A. Liu, Y. Guan, J. Zheng, Z. Shen, X. Wan, *Langmuir* **2010**, *26*, 3615–3622.
- [5] a) A. R. Hirst, D. K. Smith, M. C. Feiters, H. P. M. Geurts, *Langmuir* **2004**, *20*, 7070–7077; b) Y. Ji, Y. F. Luo, X. R. Jia, E. Q. Chen, Y. Huang, C. Ye, B. B. Wang, Q. F. Zhou, Y. Wei, *Angew. Chem.* **2005**, *117*, 6179–6183; *Angew. Chem. Int. Ed.* **2005**, *44*, 6025–6029; c) X. Yang, R. Lu, F. Gai, P. Xue, Y. Zhan, *Chem. Commun.* **2010**, *46*, 1088–1090; d) M. Seo, J. H. Kim, J. Kim, N. Park, J. Park, S. Y. Kim, *Chem. Eur. J.* **2010**, *16*, 2427–2441; e) P. Rajamalli, E. Prasad, *Org. Lett.* **2011**, *13*, 3714–3717.
- [6] a) A. Ajayaghosh, S. J. George, *J. Am. Chem. Soc.* **2001**, *123*, 5148–5149; b) S. J. George, A. Ajayaghosh, P. Jonkheijm, A. P. H. J. Schenning, E. W. Meijer, *Angew. Chem.* **2004**, *116*, 3504–3507; *Angew. Chem. Int. Ed.* **2004**, *43*, 3422–3425; c) A. Ajayaghosh, V. K. Praveen, C. Vijayakumar, S. J. George, *Angew. Chem.* **2007**, *119*, 6376–6381; *Angew. Chem. Int. Ed.* **2007**, *46*, 6260–6265; d) S. K. Samanta, A. Pal, S. Bhattacharya, *Langmuir* **2009**, *25*, 8567–8578; e) S. K. Samanta, S. Bhattacharya, *Chem. Eur. J.* **2012**, *18*, 15875–15885; f) S. Bhattacharya, S. K. Samanta, *Chem. Eur. J.* **2012**, *18*, 16632–16641; g) K. K. Kartha, R. D. Mukhopadhyay, A. Ajayaghosh, *Chimia* **2013**, *67*, 51–63.
- [7] a) C. Geiger, M. Stanescu, L. Chen, D. G. Whitten, *Langmuir* **1999**, *15*, 2241–2245; b) S. Bhowmik, S. Banerjee, U. Maitra, *Chem. Commun.* **2010**, *46*, 8642–8644.
- [8] a) M. de Loos, J. van Esch, I. Stokroos, R. M. Kellogg, B. L. Feringa, *J. Am. Chem. Soc.* **1997**, *119*, 12675–12676; b) L. A. Estroff, A. D. Hamilton, *Angew. Chem.* **2000**, *112*, 3589–3592; *Angew. Chem. Int. Ed.* **2000**, *39*, 3447–3450; c) J. J. van Gorp, J. A. J. M. Vekemans, E. W. Meijer, *J. Am. Chem. Soc.* **2002**, *124*, 14759–14769; d) F. Rodríguez-Llansola, D. Hermida-Merino, B. Nieto-Ortega, F. J. Ramírez, J. T. López Navarrete, J. Casado, I. W. Hamley, B. Escuder, W. Hayes, J. F. Miravet, *Chem. Eur. J.* **2012**, *18*, 14725–14731; e) G. O. Lloyd, M. O. M. Pipenbrock, J. A. Foster, N. Clarke, J. W. Steed, *Soft Matter* **2012**, *8*, 204–216.
- [9] a) M. Shirakawa, N. Fujita, S. Shinkai, *J. Am. Chem. Soc.* **2003**, *125*, 9902–9903; b) M. Shirakawa, S. I. Kawano, N. Fujita, K. Sada, S. Shinkai, *J. Org. Chem.* **2003**, *68*, 5037–5044; c) S. Tanaka, M. Shirakawa, K. Kaneko, M. Takeuchi, S. Shinkai, *Langmuir* **2005**, *21*, 2163–2172.
- [10] a) S. Bhattacharya, S. N. G. Acharya, A. R. Raju, *Chem. Commun.* **1996**, 2101–2102; b) S. Bhattacharya, Y. Krishnan-Ghosh, *Chem. Commun.* **2001**, 185–186; c) M. Suzuki, Y. Nakajima, T. Sato, H. Shirai, K. Hanabusa, *Chem. Commun.* **2006**, 377–379; d) A. Pal, Y. K. Ghosh, S. Bhattacharya, *Tetrahedron* **2007**, *63*, 7334–7348; e) M. Suzuki, H. Saito, H. Shirai, K. Hanabusa, *New J. Chem.* **2007**, *31*, 1654–1660; f) B. Adhikari, J. Nanda, A. Banerjee, *Chem. Eur. J.* **2011**, *17*, 11488–11496; g) J. Raeburn, T. O. McDonald, D. J. Adams, *Chem. Commun.* **2012**, *48*, 9355–9357; h) V. J. Nebot, J. Armengol, J. Smets, S. F. Prieto, B. Escuder, J. F. Miravet, *Chem. Eur. J.* **2012**,

- 18, 4063–4072; i) S. Datta, S. K. Samanta, S. Bhattacharya, *Chem. Eur. J.* **2013**, *19*, 11364–11373.
- [11] M. Durkut, M. M. -Torrent, P. Hadley, P. Jonkheijm, A. P. H. J. Schenning, E. W. Meijer, S. George, A. Ajayaghosh, *J. Chem. Phys.* **2006**, *124*, 154704–154710.
- [12] D. González-Rodríguez, P. G. A. Janssen, R. Martín-Rapún, I. De Cat, S. De Feyter, A. P. H. J. Schenning, E. W. Meijer, *J. Am. Chem. Soc.* **2010**, *132*, 4710–4719.
- [13] a) S. Srinivasan, S. S. Babu, V. K. Praveen, A. Ajayaghosh, *Angew. Chem.* **2008**, *120*, 5830–5833; *Angew. Chem. Int. Ed.* **2008**, *47*, 5746–5749; b) S. Srinivasan, V. K. Praveen, R. Philip, A. Ajayaghosh, *Angew. Chem.* **2008**, *120*, 5834–5838; *Angew. Chem. Int. Ed.* **2008**, *47*, 5750–5754; c) S. K. Samanta, A. Pal, S. Bhattacharya, C. N. R. Rao, *J. Mater. Chem.* **2010**, *20*, 6881–6890; d) S. K. Samanta, K. S. Subrahmanyam, S. Bhattacharya, C. N. R. Rao, *Chem. Eur. J.* **2012**, *18*, 2890–2901.
- [14] a) J. A. Sáez, B. Escuder, J. F. Miravet, *Chem. Commun.* **2010**, *46*, 7996–7998; b) S. Datta, S. Bhattacharya, *Chem. Commun.* **2012**, *48*, 877–879; c) A. Reddy, A. Sharma, A. Srivastava, *Chem. Eur. J.* **2012**, *18*, 7575–7581; d) R. N. Das, Y. P. Kumar, S. Pagoti, A. J. Patil, J. Dash, *Chem. Eur. J.* **2012**, *18*, 6008–6014; e) W. A. Velema, M. C. A. Stuart, W. Szymanski, B. L. Feringa, *Chem. Commun.* **2013**, *49*, 5001–5003; f) J. Boekhoven, J. M. Poolam, C. Maity, F. Li, L. van der Mee, C. B. Minkenberg, E. Mendes, J. H. van Esch, R. Eelkema, *Nat. Chem.* **2013**, *5*, 433–437; g) C. B. Minkenberg, W. D. Hendriksen, F. Li, E. Mendes, R. Eelkema, J. H. van Esch, *Chem. Commun.* **2012**, *48*, 9837–9839; h) B. G. Bag, R. Majumdar, S. K. Dinda, P. P. Dey, G. C. Maity, V. A. Mallia, R. G. Weiss, *Langmuir* **2013**, *29*, 1766–1778.
- [15] a) Z. Yang, K. Xu, L. Wang, H. Gu, H. Wei, M. Zhang, B. Xu, *Chem. Commun.* **2005**, 4414–4416; b) J. Zhang, S. Chen, S. Xiang, J. Huang, L. Chen, C. Y. Su, *Chem. Eur. J.* **2011**, *17*, 2369–2372; c) T. Ishiwata, Y. Furukawa, K. Sugikawa, K. Kokado, K. Sada, *J. Am. Chem. Soc.* **2013**, *135*, 5427–5432.
- [16] a) Z. Yang, B. Xu, *J. Mater. Chem.* **2007**, *17*, 2385–2393; b) F. Zhao, M. L. Ma, B. Xu, *Chem. Soc. Rev.* **2009**, *38*, 883–891; c) B. Roy, A. Saha, A. Esterrani, A. K. Nandi, *Soft Matter* **2010**, *6*, 3337–3345.
- [17] a) H. Ihara, T. Sakurai, T. Yamada, T. Hashimoto, M. Takafuji, T. Sagawa, H. Hachisako, *Langmuir* **2002**, *18*, 7120–7123; b) Q. Liu, Y. Wang, W. Li, L. Wu, *Langmuir* **2007**, *23*, 8217–8223; c) K. N. King, A. J. McNeil, *Chem. Commun.* **2010**, *46*, 3511–3513; d) P. Byrne, G. O. Lloyd, L. Applegarth, K. M. Anderson, N. Clarke, J. W. Steed, *New J. Chem.* **2010**, *34*, 2261–2274; e) M.-O. M. Piepenbrock, G. O. Lloyd, N. Clarke, J. W. Steed, *Chem. Rev.* **2010**, *110*, 1960–2004.
- [18] a) K. Hanabusa, T. Miki, Y. Taguchi, T. Koyama, H. Shirai, *J. Chem. Soc. Chem. Commun.* **1993**, 1382–1384; b) K. Inoue, Y. Ono, Y. Kanekiyo, T. Ishi-i, K. Yoshihara, S. Shinkai, *J. Org. Chem.* **1999**, *64*, 2933–2937; c) M. de Loos, J. V. Esch, R. M. Kellogg, B. L. Feringa, *Angew. Chem.* **2001**, *113*, 633–636; *Angew. Chem. Int. Ed.* **2001**, *40*, 613–616; d) B. A. Simmons, C. E. Taylor, F. A. Landis, V. T. John, G. L. McPherson, D. K. Schwartz, R. Moore, *J. Am. Chem. Soc.* **2001**, *123*, 2414–2421; e) S. Manna, A. Saha, A. K. Nandi, *Chem. Commun.* **2006**, 4285–4287; f) S. Mahesh, R. Thirumalai, S. Yagai, A. Kitamura, A. Ajayaghosh, *Chem. Commun.* **2009**, 5984–5986; g) L. Meazza, J. A. Foster, K. Fucke, P. Metrangolo, G. Resnati, J. W. Steed, *Nat. Chem.* **2013**, *5*, 42–47.
- [19] a) U. Maitra, P. V. Kumar, N. Chandra, L. J. D'Souza, M. D. Prasanna, A. R. Raju, *Chem. Commun.* **1999**, 595–596; b) A. Friggeri, O. Gronwald, K. J. C. van Bommel, S. Shinkai, D. N. Reinhoudt, *J. Am. Chem. Soc.* **2002**, *124*, 10754–10758; c) J. R. Moffat, D. K. Smith, *Chem. Commun.* **2008**, 2248–2250; d) M. R. Molla, S. Ghosh, *Chem. Eur. J.* **2012**, *18*, 9860–9869; e) K. V. Rao, S. J. George, *Chem. Eur. J.* **2012**, *18*, 14286–14291.
- [20] a) M. George, R. G. Weiss, *Langmuir* **2002**, *18*, 7124–7135; b) M. George, R. G. Weiss, *Langmuir* **2003**, *19*, 1017–1025; c) M. Ayabe, T. Kishida, N. Fujita, K. Sada, S. Shinkai, *Org. Biomol. Chem.* **2003**, *1*, 2744–2747; d) D. R. Trivedi, A. Ballabh, P. Dastidar, *Chem. Mater.* **2003**, *15*, 3971–3973; e) A. Pal, H. Basit, S. Sen, V. K. Aswal, S. Bhattacharya, *J. Mater. Chem.* **2009**, *19*, 4325–4334; f) P. Sahoo, R. Sankolli, H. Y. Lee, S. R. Raghavan, P. Dastidar, *Chem. Eur. J.* **2012**, *18*, 8057–8063; g) H. Basit, A. Pal, S. Sen, S. Bhattacharya, *Chem. Eur. J.* **2008**, *14*, 6534–6545; h) W. Edwards, D. K. Smith, *J. Am. Chem. Soc.* **2013**, *135*, 5911–5920.
- [21] a) S. Bhattacharya, A. Srivastava, A. Pal, *Angew. Chem.* **2006**, *118*, 3000–3003; *Angew. Chem. Int. Ed.* **2006**, *45*, 2934–2937; b) A. Pal, A. Srivastava, S. Bhattacharya, *Chem. Eur. J.* **2009**, *15*, 9169–9182.
- [22] a) S. K. Samanta, S. Bhattacharya, *Chem. Commun.* **2013**, *49*, 1425–1427; b) P. Xue, Q. Xu, P. Gong, C. Qian, A. Ren, Y. Zhang, R. Lu, *Chem. Commun.* **2013**, *49*, 5838–5840.
- [23] S. Babić, A. J. M. Horvat, D. M. Pavlović, M. K. Kaštelan-Macan, *TrAC Trends Anal. Chem.* **2007**, *26*, 1043–1061.
- [24] a) S. Mohamed, D. A. Tocher, M. Vickers, P. G. Karamertzanis, S. L. Price, *Cryst. Growth Des.* **2009**, *9*, 2881–2889; b) B. R. Bhogala, S. Basavoju, A. Nangia, *CrystEngComm* **2005**, *7*, 551–562.
- [25] H. Mishra, S. Enami, R. J. Nielsen, L. A. Stewart, M. R. Hoffmann, W. A. Goddard, A. J. Colussi, *Proc. Natl. Acad. Sci. USA* **2012**, *109*, 18679–18683.
- [26] a) P. Gao, C. Zhan, L. Liu, Y. Zhou, M. Liu, *Chem. Commun.* **2004**, 1174–1175; b) D. L. Allara, R. G. Nuzzo, *Langmuir* **1985**, *1*, 52–56.
- [27] Y. Furukawa, T. Ishiwata, K. Sugikawa, K. Kokado, K. Sada, *Angew. Chem.* **2012**, *124*, 10718–10721; *Angew. Chem. Int. Ed.* **2012**, *51*, 10566–10569.
- [28] a) S. J. George, Ž. Tomović, M. M. J. Smulders, T. F. A. de Greef, P. E. L. G. Leclere, E. W. Meijer, A. P. H. J. Schenning, *Angew. Chem.* **2007**, *119*, 8354–8359; *Angew. Chem. Int. Ed.* **2007**, *46*, 8206–8211; b) S. J. George, R. de Bruijn, Z. Tomović, B. V. Averbek, D. Beljonne, R. Lazzaroni, A. P. H. J. Schenning, E. W. Meijer, *J. Am. Chem. Soc.* **2012**, *134*, 17789–17796.
- [29] M. M. J. Smulders, M. M. L. Nieuwenhuizen, T. F. A. de Greef, P. van der Schoot, A. P. H. J. Schenning, E. W. Meijer, *Chem. Eur. J.* **2010**, *16*, 362–367.
- [30] a) T. Kato in *Handbook of Liquid Crystals, Vol. 2B* (Eds.: D. Demus, J. Goodby, J. W. Gray, H.-W. Spiess, V. Vill), Wiley-VCH, Weinheim, **1998**, pp. 969–979; b) J. F. Eckert, U. Maciejczuk, D. Guillon, J. F. Nierengarten, *Chem. Commun.* **2001**, 1278–1279.
- [31] a) N. V. S. Rao, R. Deb, M. K. Paul, T. Francis, *Liq. Cryst.* **2009**, *36*, 977–987; b) A. Wicklein, P. Kohn, L. Ghazaryan, T. T. Albrecht, M. Thilakkat, *Chem. Commun.* **2010**, *46*, 2328–2330; c) L. Chakraborty, N. Chakraborty, T. D. Choudhury, B. V. N. P. Kumar, A. B. Mandal, N. V. S. Rao, *Liq. Cryst.* **2012**, *39*, 655–668.
- [32] F. S. Precup-Blaga, A. P. H. J. Schenning, E. W. Meijer, *Macromolecules* **2003**, *36*, 565–572.
- [33] U. K. Das, P. Dastidar, *Chem. Eur. J.* **2012**, *18*, 13079–13090.

Received: June 2, 2013

Revised: September 9, 2013

Published online: November 5, 2013